Spring 2018

Molecular Organization of Vapor Deposited Rod-Like Molecules

Andrew Audley
aja78@zips.uakron.edu

Molecular Organization of Vapor Deposited Rod-Like Molecules

A Thesis

Presented to

The Williams Honors College

of

The University of Akron

Andrew Audley

April, 2018

Abstract

Thiophenes are π-conjugated organic molecules with applications in electronic devices. Alpha-sexithiophene (α-6T) is a rod-like molecule consisting of six thiophene rings. Previous experimental research has shown that vapor deposition of rod-like organic molecules onto substrates at different temperatures yields films with a range of phases. These include smectic liquid crystalline phases, which have been shown to promote anisotropic charge carrier mobility. In this work, we use a course-grained model for α-6T, representing it as a chain of discotic particles with fixed bond lengths and fixed bond angles. We perform Monte Carlo simulations of multiple chains introduced at different rates in vacuum near two adsorbing surfaces. These simulations are not chemically realistic, instead focusing on the general features of the physical systems. The goal of this work is to simulate vapor deposition of materials on a substrate over a range of temperatures and deposition rates and to investigate the resulting structures.

Table of Contents

1   Introduction

Liquid crystals are materials with properties of both liquids and crystalline solids. Molecules in a liquid crystal exhibit liquid-like ordering as well as anisotropy in one or three dimensions [1]. Liquid crystals may exhibit a number of phases under different conditions. Illustrations of the crystalline, nematic, and isotropic phases are shown in Figure 1.1. Nematic and layered smectic phases are of particular interest, as their presence in materials have been shown to promote anisotropic charge carrier mobility. [2] [3] [4] In the nematic phase, the axes of the molecules in a liquid crystal align themselves with a particular direction. In this work, we will be focusing on chain-like molecules that are stiff enough to behave like rods.
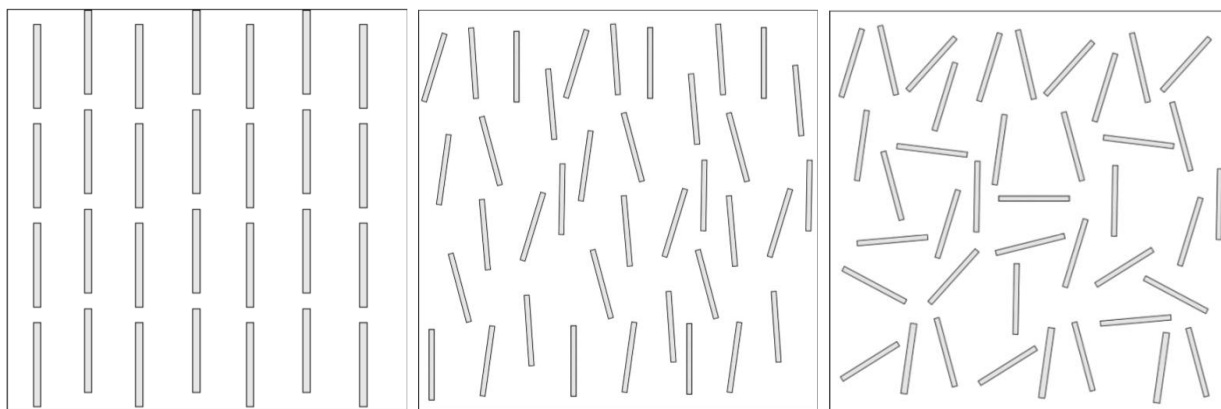
Figure 1.1 Left to right: Crystalline, nematic, and isotropic liquid crystalline phases for rod-like molecules, image from Ref. [5].

In recent experiments, Gujral *et al*. [6] observed liquid crystalline phases in vapor deposited layers of itraconazole, a rod-like organic molecule known to be a good glass former. In these experiments, glassy layers were produced in samples of vapor deposited itraconazole with structures that depend on substrate temperature. At low temperatures, itraconazole glasses were found to exhibit amorphous material phases, while at higher temperatures smectic-like layering was observed, as shown in Figure 1.2.

Thiophenes are ring-shaped organic semiconducting molecules with applications in low cost electronic devices. When connected as a chain of six rings, these molecules become $\alpha-$sexithiophene (α-6T), shown in Figure 1.3. Simulations by Pizzirusso *et al.* [7] have shown that this molecule exhibits crystalline, liquid crystalline, and nematic phases in bulk material. In
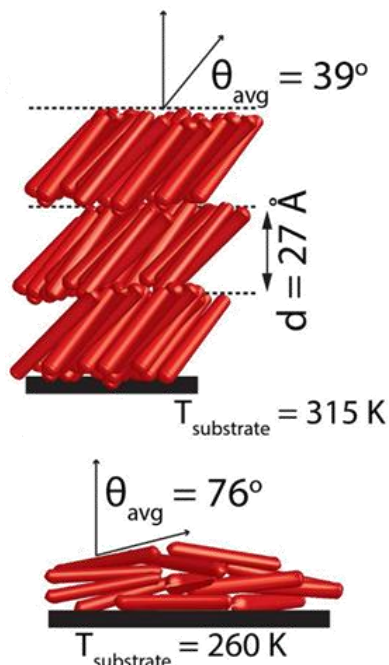
Figure 1.2 Top: Itraconazole molecules deposited onto a substrate at 315 K, exhibiting smectic-like layers. Bottom: Itraconazole deposited onto a substrate at 260K, exhibiting the amorphous material phase. Image from Ref. [6].
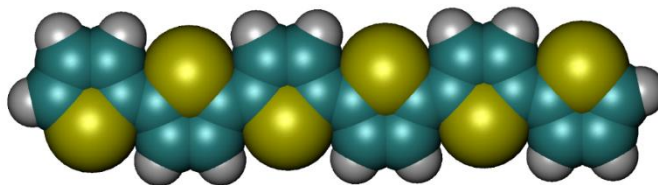
Figure 1.3 A single chain of α-6T, with white, teal, and yellow spheres representing hydrogen, carbon, and sulfur, respectively.

simulations by Garcia [5], surface behavior for single chains and monolayers of α-6T were investigated over a range of temperatures. Figure 1.4 shows the nematic order parameter, S, as a function of reduced temperature for simulations of α−6T molecules near a gold surface. At low temperatures ($T_{red} < 0.9$), the molecules form a densely packed single layer. At high temperatures, they spread out to a layer of low surface density. At low temperature, $S \cong 1.0$, indicating orientational order of the chains in this region. As temperature is increased, S drops sharply at $T_{red} = 0.9$, reaching a value of approximately 0.325 at $T_{red} = 1.0$. In this mid-
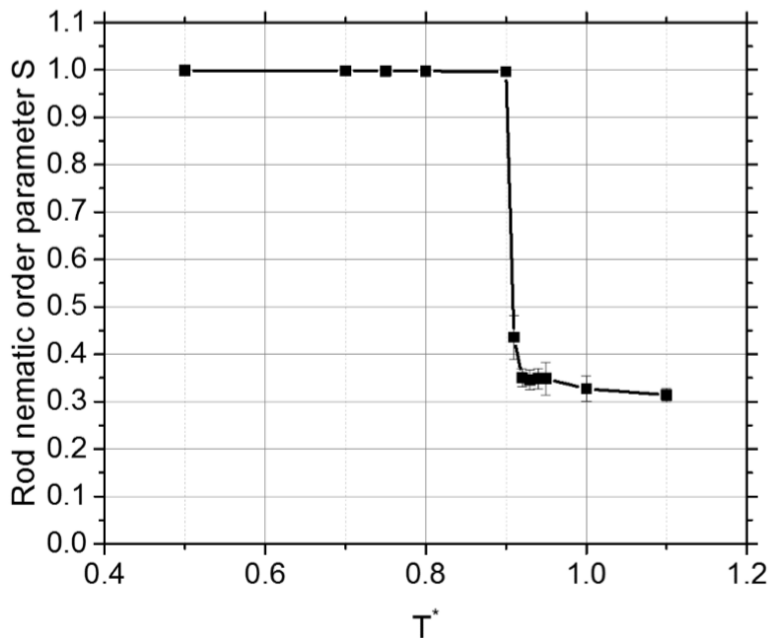
Figure 1.4 Nematic order parameter, S, as a function of reduced temperature, here given by T*. The figure shows simulation results of α-6T near a smooth surface, from Ref. [5].

temperature region, the molecules are no longer ordered. For high temperatures, $T_{red} \geq 1.5$, the molecules are not expected to show any order.

In this work, we are primarily concerned with the behaviors of chains in sub-monolayer, monolayer, and more-than-a-monolayer conformations, where a monolayer denotes a conformation in which molecules fill the first layer above the surface.

Simulations in this work are performed using the Metropolis Monte Carlo method. In Monte Carlo simulations of this type, a selection of moves is defined which are applied in random fashion to the constituent elements of a model, altering the configuration of the system and thereby its energy. The energies of the configurations before and after each move are compared, and new configurations are accepted when they satisfy the Metropolis acceptance criterion described in section 3.

In the following section, section 2, we introduce our model for α-6T molecules. This is followed by a description of our simulation method in section 3. We present and discuss our results in section 4 and provide a summary and conclusions in section 5.

6

2   Model

In this work, we use a coarse-grained representation of thiophene, choosing to represent each ring as a discotic bead. The diameter and height of each bead are defined as $\sigma_e = 6.3105$ Å and $\sigma_f = 0.5\ \sigma_e$, respectively. A factor of σ_0 is a useful length scale in this work, with $\sigma_0 = \sigma_e$. Each α-6T molecule in this model is represented as a chain of six overlapping beads, with each bead connected to its neighbors by bonds of fixed length, b, as measured from the center of each bead. Neighboring beads have a fixed bond angle, θ_0, as well. Each bead has an orientation vector, $\hat{u}$, which is parallel to the shortest axis through the body of the bead and perpendicular to the bonds connecting the bead to its neighbor. Figure 2.1 shows a coarse-grained representation of a single molecule of α-6T.
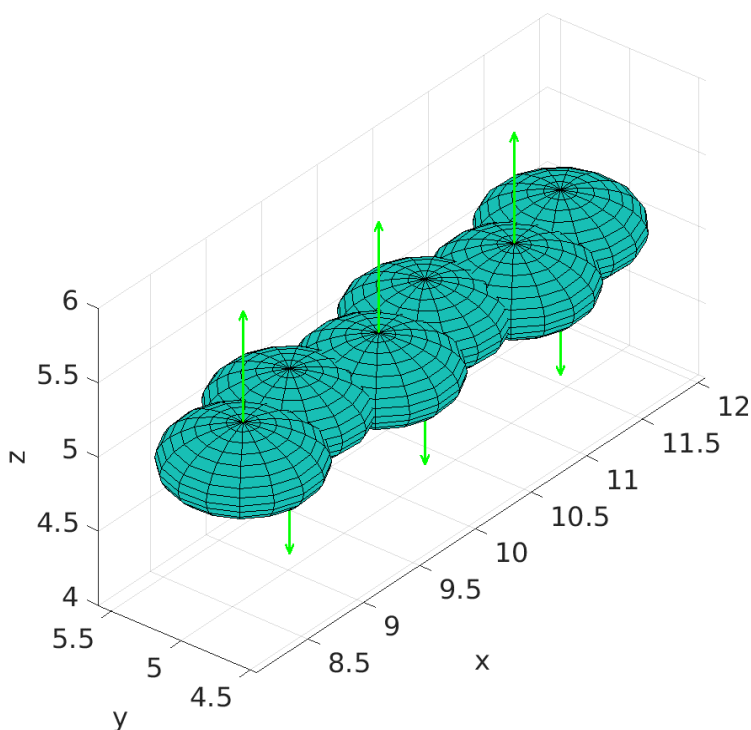
Figure 2.1 A single molecule of α-6T in coarse-grained representation. The ellipsoids show the discotic beads representing the rings of the molecule. The green arrow projected from the surface of each bead shows the orientation vector for that bead. In this configuration, the orientation vectors for neighboring beads have opposite directions. This is the configuration with the lowest dihedral energy.

Each bead is allowed to rotate about the bond vectors in the chain, with corresponding changes in configuration controlled by a dihedral potential [8]

7

$$U_{\text{dihedral}}(\varphi_{ij}) = \sum_{n=1}^{N_{\text{bead}}-1} U_d(\varphi_{i,i+1}), \tag{1}$$

with

$$U_d(\varphi_{ij}) = \sum_{n=1}^{5} c_n (\cos(\varphi))^n, \tag{2}$$

where $N_{\text{bead}} = 6$ is the number of beads in a chain, and φ_{ij} is the angle between the orientation vectors $\hat{\mathbf{u}}_i$ and $\hat{\mathbf{u}}_j$ of neighboring beads. The coefficients c_n used in this work are given in Table 1. When neighboring beads have opposing orientations, the dihedral potential between them is minimized.

Table 1 Values of c_n used in this work, from Ref. [5].

c_n	Value
c_1	3.571 kcal/mol
c_2	-0.2819 kcal/mol
c_3	-5.497 kcal/mol
c_4	0.7049 kcal/mol
c_5	2.349 kcal/mol

Beads in separate chains interact with one another through a Gay-Berne potential for ellipsoidal molecules. This potential is given as a function of orientation vectors $\hat{\mathbf{u}}_i$ and $\hat{\mathbf{u}}_j$ of the interacting beads and the displacement vector, $\mathbf{r}$, between them. The equation for this potential is [5] [8] [9]

$$U_{\text{GB}}(\hat{u}_j, \hat{u}_j, \mathbf{r}) = 4\epsilon(\hat{u}_j, \hat{u}_j, \mathbf{r})\left[\left(\frac{\sigma_f}{r - \sigma(\hat{u}_j, \hat{u}_j, \mathbf{r}) + \sigma_f}\right)^{12} - \left(\frac{\sigma_f}{r - \sigma(\hat{u}_j, \hat{u}_j, \mathbf{r}) + \sigma_f}\right)^{6}\right]. \tag{3}$$

To help interpret this potential, Figure 2.2 shows the Gay-Berne potential as a function of distance for three configurations of two beads.
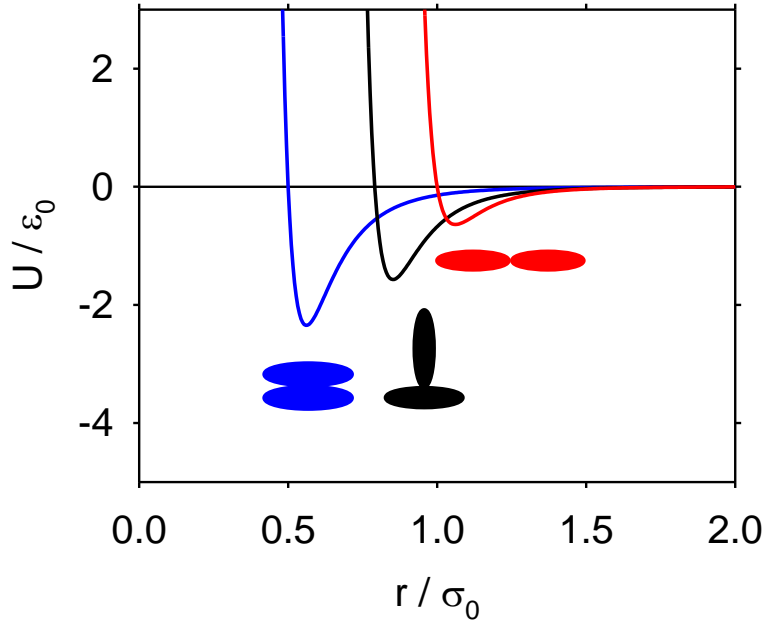
Figure 2.2 The Gay-Berne potential between two beads as a function of center-to-center distance. Potential curves for the face-to-face (blue), edge-to-face (black), and edge-to-edge (red) configurations are shown. Image from Ref. [5].

In this work, α−6T chains are injected into a box with dimensions L_x, L_y, and L_z. In all simulations, we use periodic boundary conditions in the x and y directions and attractive, impenetrable surfaces at the floor and ceiling; an example is shown in Figure 2.3. Three different sizes are used in this work: a large box with $L_x = 20.1\sigma_0$, $L_y = 20.1\sigma_0$, and $L_z = 20\sigma_0$; a medium box with dimensions $L_x = 20.1\sigma_0$, $L_y = 20.1\sigma_0$, and $L_z = 10\sigma_0$, and a small box with dimensions $L_x = 20.1\sigma_0$, $L_y = 10.05\sigma_0$, and $L_z = 10\sigma_0$. Using smaller boxes allows us to more quickly adsorb chains, as they have to travel less distance to find the surfaces.

Beads in the chains interact with the adsorbing surfaces with a potential given by [10]

$$U_{\text{wall}}(z,\theta) = \epsilon_w \left[\frac{2}{15}\left(\frac{\sigma_f}{z - z_{shift}(\theta)}\right)^9 - \left(\frac{\sigma_f}{z - z_{shift}(\theta)}\right)^3 \right] \times (1 + AP_2[\cos(\theta)]), \qquad (4)$$

where

$$z_{\text{shift}}(\theta) = 0.5 \left[\sigma_0 \left(1 - \frac{2\chi}{1+\chi} \cos^2\theta \right)^{-\frac{1}{2}} - \sigma_f \right],$$ (5)

θ is the angle between the orientation vector and the normal vector of the adsorbing surface, $A = 1$, $\epsilon_w = 14\epsilon_0$, and $P_2[\cos(\theta)] \equiv P_2[x] = \frac{1}{2}(3x^2 - 1)$ is the second order Legendre polynomial.
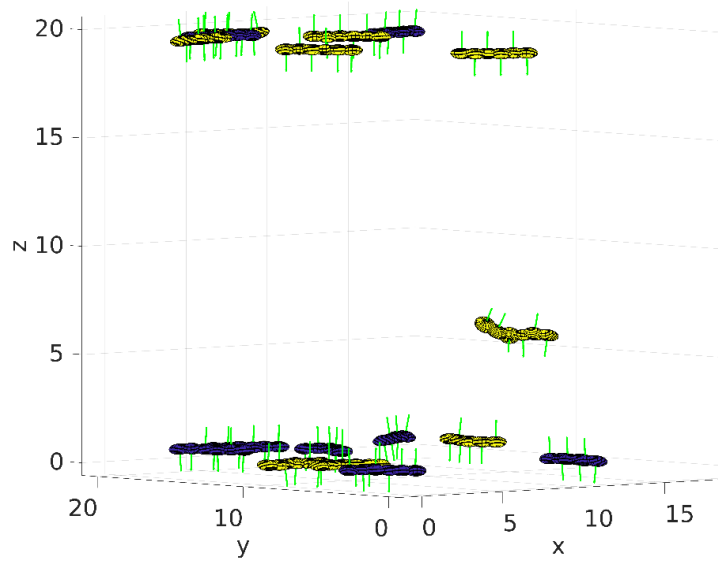
Figure 2.3 Example of a simulation box. This figure shows a snapshot of the simulation in the large box. Notice how the chains at the floor and ceiling of the box have attached to the adsorbing surfaces. One chain in the lower right can be seen in midflight before it finds the surface.

The term χ in equation (5) is defined as

$$\chi = \frac{(\kappa)^2 - 1}{(\kappa)^2 + 1},$$ (6)

with

$$\kappa = \frac{\sigma_f}{\sigma_e} = 0.5.$$ (7)

The surface potential is visualized in Figure 2.4.

10

The total energy of the system is a combination of all three of the aforementioned potentials

$$U = \sum_{i=1}^{N} U_{\text{dih}} + \sum_{i=1}^{N} U_{\text{wall}} + \frac{1}{2} \sum_{i=1}^{N_{\text{dih}}N} \sum_{j=1}^{N_{\text{dih}}N} U_{GB}(\hat{u}_j, \hat{u}_j, \mathbf{r}). \tag{8}$$

The unit for energy in this work is $\epsilon_0 = 0.54$ kcal/mol, and the reduced temperature is given by

$$T_{\text{red}} = \frac{k_B T}{\epsilon_0}, \tag{9}$$

where k_B is Boltzmann's constant.
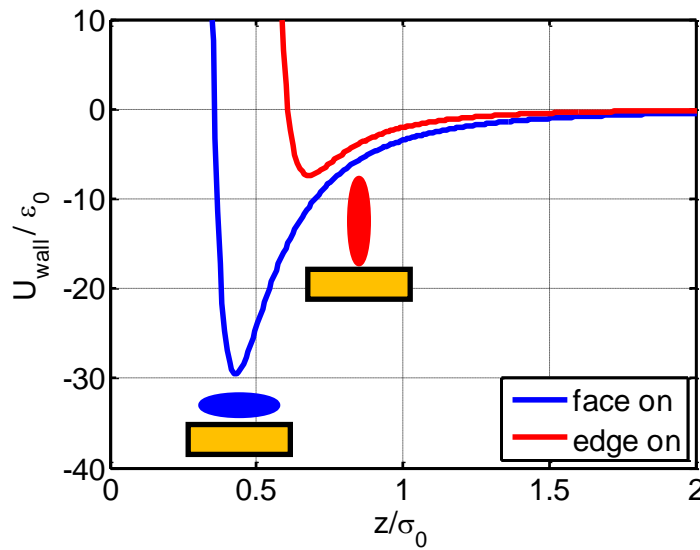
Figure 2.4 The potential energy of a bead near an adsorbing surface as a function distance. Potential curves for the face on (blue) and edge on (red) configurations are shown.

3   Method

In this work, we perform Monte Carlo simulations for a variable number, N, of α-6T chains injected one-by-one into the center of a box described in the Model section. Over a prescribed number of Monte Carlo steps, mc, each chain in the box was subjected to a set of randomized moves. Each move alters the configuration of the system, thereby changing the total energy of the system. The energy of the system after the move, E_{fin}, is compared to the energy of the system before the move, E_{ini}. These simulations are carried out in the canonical ensemble, in which new configurations are accepted with a probability, p, given the Metropolis criterion:

$$p = \begin{cases} e^{-(E_{fin}-E_{ini})\beta}, & E_{fin} > E_{ini} \\ 1, & E_{fin} \leq E_{ini} \end{cases}, \tag{10}$$

with

$$\beta = \frac{1}{k_B T} = (\epsilon_0 T_{red})^{-1}. \tag{11}$$

Three different moves are used in our simulation: rigid translations of the chains in three dimensions, rigid rotations of the chains about their three principal axes, and pivot moves, in which beads within chains rotate about their bonds. A single Monte Carlo step consists of one of each of these moves, carried out in random order for each chain in the box. During each simulation, accepted configurations are written to a trajectory file on a prescribed interval for later evaluation.

Our simulations begin with a single chain in the center of the box, allowed to move with probability. At a prescribed rate, a new chain is injected into the center of the box. For our simulation, these rates range from one new chain every 5,000 Monte Carlo steps to one every 50,000 Monte Carlo steps.

Results for our simulations are evaluated from the trajectory file which contains the positions and orientations of all beads as well as the total energy of the configuration. These data are used to evaluate the average surface potential per bead, the average total energy per bead, and the average distance from an adsorbing surface of the chains over the duration of the simulations. Furthermore, the probability distribution for finding a chain at a given height is extracted from

the trajectory file. Using this probability distribution, the number of molecules in each deposited layer can be estimated. Furthermore, the area density of each layer can be approximated to give a better understanding of the packing of α-6T near the surfaces. A list of parameters for all simulations evaluated in this work is presented in Table 2.

T_{red}	L_x (σ_0)	L_y (σ_0)	L_z (σ_0)	Final N	Inverse Rate (MC steps)	Estimated Coverage	Simulation time (MC steps)
0.50	20.10	20.10	20.0	100	50000	Less than a monolayer	6.00E+06
0.75	20.10	10.05	10.0	100	25000	Approx. a monolayer	3.00E+06
0.75	20.10	10.05	10.0	200	10000	More than a monolayer	3.00E+06
0.75	20.10	10.05	10.0	300	10000	More than a monolayer	4.00E+06
0.75	20.10	10.05	10.0	400	10000	More than a monolayer	5.00E+06
1.00	20.10	20.10	20.0	100	50000	Less than a monolayer	6.00E+06
1.50	20.10	20.10	20.0	100	50000	Less than a monolayer	6.00E+06
1.50	20.10	20.10	10.0	250	50000	More than a monolayer	1.40E+07
1.50	20.10	20.10	10.0	250	50000	More than a monolayer	1.40E+07
1.50	20.10	20.10	10.0	250	50000	More than a monolayer	1.40E+07
1.50	20.10	20.10	10.0	250	50000	More than a monolayer	1.40E+07

Table 2 Parameters for the simulations discussed in this work. The columns in this table give, from left to right, the reduced temperature, the box dimensions, the total number of molecules, the deposition rate (one particle every x Monte Carlo steps), estimated surface coverage, and simulation time used in each simulation.

4   Results and Discussion

In this work, simulations are performed for systems forming layers of varying thickness from less than a monolayer up to more than two layers. The simulation parameters are presented in Table 2. The most important parameters for the final structure are temperature and deposition rate. We are interested in the average distance from the substrate, Z_{dist}, the average energy per bead, U_{bead}, and the average surface potential energy, U_{wall}, as a function of simulation time measured in Monte Carlo steps. The probability distribution for the molecules with respect to height is also evaluated, as well as the ordering of the molecules, especially in the first layer.

4.1   Sub-monolayers at different temperatures

We first investigate deposition behavior for simulations of $N = 100$ chains, with a deposition rate of one new chain every 50,000 Monte Carlo steps, the bottom four simulations in Table 2. For these simulation $L_{\text{x}} = 20.1\sigma_0$, $L_{\text{y}} = 20.1\sigma_0$, and $L_{\text{z}} = 20\sigma_0$. The final configurations for this number of molecules have less than a monolayer of molecules deposited onto the substrate. Thus, all molecules have the opportunity to achieve their lowest energy configurations. Differences in behavior as a function of temperature were investigated for this set of simulations. Figure 4.1 and 4.2 show the average energy per bead and the average distance of the chains from the surface as a function of simulation time, for reduced temperatures of 0.5, 1.0, and 1.5.

For the simulations at $T_{\text{red}} = 0.5$, both the average energy and the average distance from an adsorbing surface show a peak early in the simulation. These peaks are the result of several chains in the box having not yet found the adsorbing surfaces, leaving them at higher energies. Investigation of the trajectory of the molecules showed that clusters of chains form early in the simulations, as shown in Figure 4.3. These clusters reduce the mobility of the chains so that they find the adsorbing surfaces later than usual. Without surface contacts, these chains are left at higher energies than those adsorbed. Over time, the clusters dissolve onto the substrates and we can see that the average energy and average surface distance fall as the chains find the surface. The final configuration presented in Figure 4.4 shows that the molecules lie flat, with opposing dihedral orientation between neighboring beads. This result is the lowest possible energy configuration for the system. When we look at Figure 4.4, we can observe the ordering of the

14

chains on the bottom surface of the box. The molecules form clusters of aligned chains in close contact.
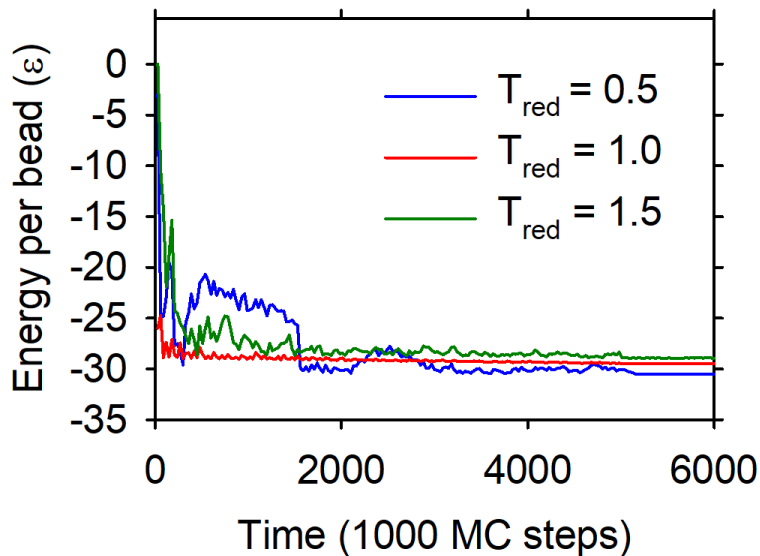
Figure 4.1 Average total energy per bead for as afunction of simulation time for $N = 100$ chains. The graphs show simulation results for reduced temperatures of 0.5 (blue), 1.0 (red), and 1.5 (green).
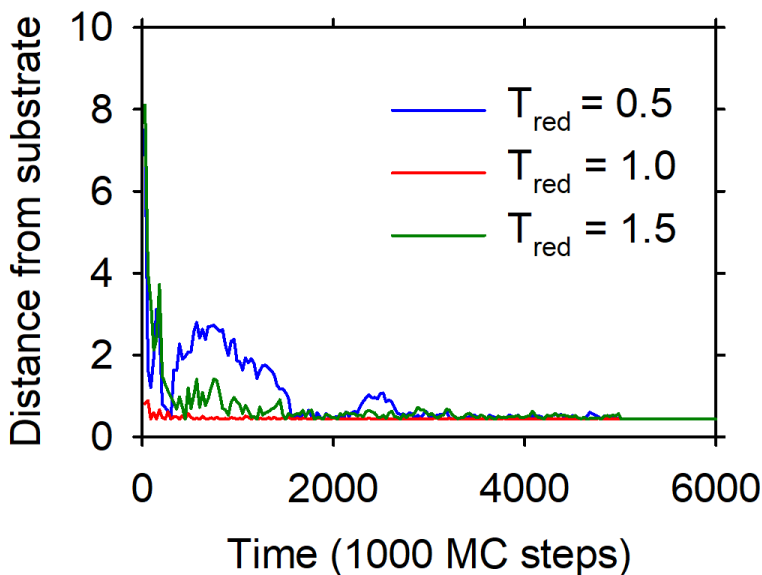
Figure 4.2 Average distance of chains from an adsorbing surface as a function of simulation time for $N = 100$ chains. The graphs show simulation results for reduced temperatures of 0.5 (blue), 1.0 (red), and 1.5 (green).

15
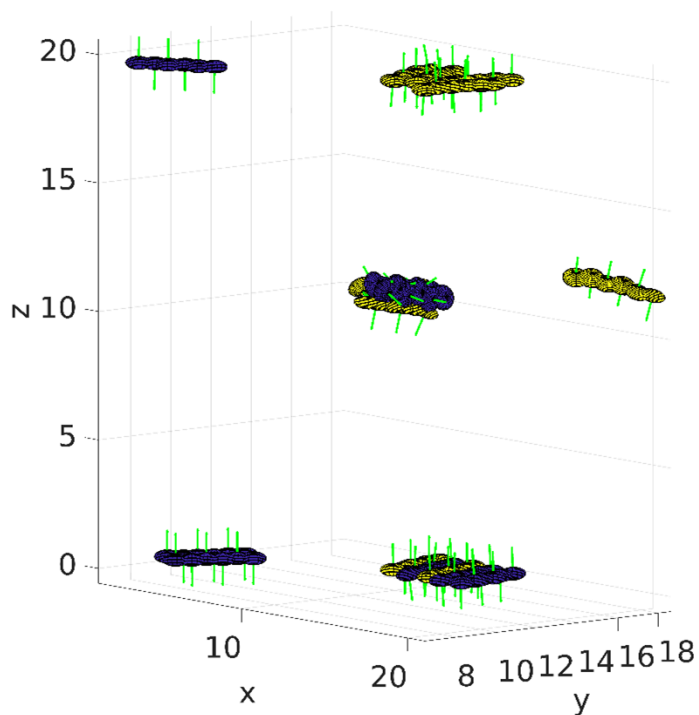
Figure 4.3 Snapshot of an early configuration of a simulation with a final number of $N = 100$ chains at $T_{\text{red}} = 0.5$. A cluster of three chains is visible in the center of the box.
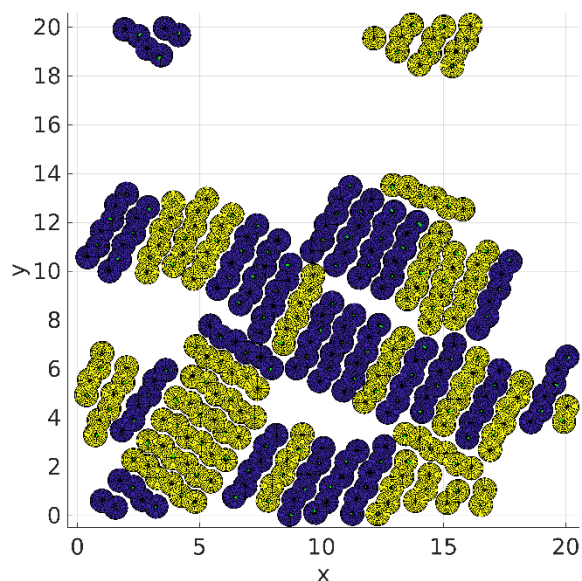
Figure 4.4 Final configuration for a sub-monolayer of α-6T molecules deposited onto a substrate at $T_{\text{red}} = 0.5$. This image shows ordering of the molecules on the surface. Notice the opposing dihedral orientations between neighboring beads in the chains.

16

Our mid temperature simulations offer a different behavior. Figures 4.1 and 4.2 show that the average energy and surface distance for the chains fall rapidly early in the simulations and then remain constant at low values. The higher temperature used in this simulation discourages the clumping of chains in the gas phase found at lower temperatures. The final configuration in Figure 4.5 shows that $T_{red} = 1.0$ is sufficiently low for the chains at the adsorbing surfaces to lie flat in low energy configurations. However, they do not form ordered clusters like the chains in the low temperature simulations did. The molecules show orientational order with their long axes pointing preferentially in one direction. Furthermore, the curved shape of some molecules shows that, for this temperature, not all neighboring beads have opposite orientation. In addition, the molecules do not touch as often as they do at $T_{red} = 0.5$. This means that there are fewer negative contributions to the energy due to the interactions between chains. The final average energy for this configuration is therefore somewhat higher than for Tred = 0.5.
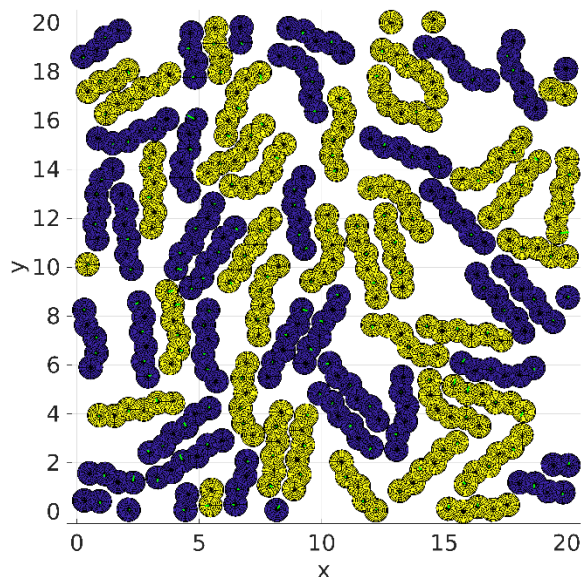
Figure 4.5 Final configuration for a sub-monolayer of α-6T molecules deposited onto a substrate at $T_{red} = 1.0$. At this temperature, the molecules do not show positional order but they have orientational order along the y-axis. Individual molecules have bent shapes, indicating that some neighboring disk orientation vectors point in the same direction.

Finally, we consider our high temperature simulations. For $T_{red} = 1.5$, Figures 4.1 and 4.2 show that the average energy per bead and the average distance from the substrate fall more rapidly than for $T_{red} = 0.5$ and less rapidly than for $T_{red} = 1.0$. As the temperature of the simulations is increased, new moves are accepted with greater and greater probability. This means that, even

though no clumps form in the box, the average energy of the system may take longer to decrease than for somewhat lower temperatures. Similarly, during the simulations the probability for a configuration with a higher energy than the previous configuration to be accepted increases. Thus, orientation vectors of neighboring beads are even less likely to be in opposite directions than for T_{red} = 1.0. This leads to a large number of bent molecules in the final configuration, shown in Figure 4.6. In addition, the molecules are spread out more than in Figure 4.5, leading to fewer contacts between chains. As a result, this final configuration has the highest final average energy of the three considered in this comparison.
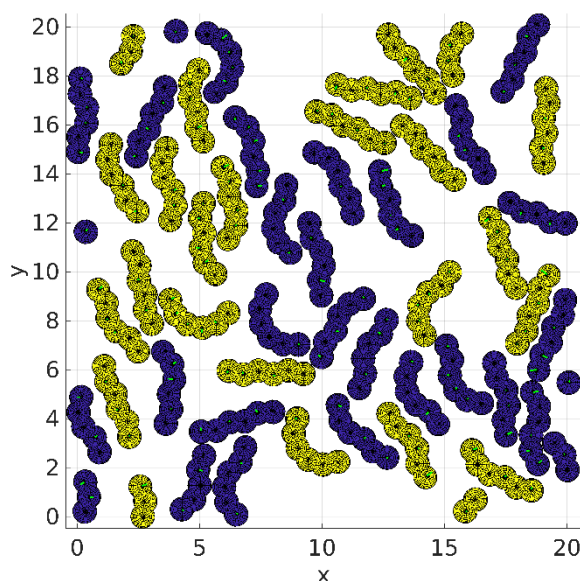
Figure 4.6 Final configuration for a sub-monolayer of α-6T molecules deposited onto a substrate at T_{red} = 1.5. At this temperature, there is only a little orientational order in the layer.

4.2   Between one and two monolayers at high temperature

In this section, we study systems with a final coverage between one and two monolayers. We performed simulations of N = 250 chains deposited at T_{red} = 1.5 with a rate of one new chain every 25,000 Monte Carlo steps. These simulations used the medium sized box which has a lower height, L_z = 10, in order to encourage quick adsorption of the molecules. The total simulation time was 1.4×10^7 Monte Carlo steps. Since the final configurations have more than one monolayer of molecules on each adsorbing surface, we are able to investigate the onset of growth in the second layer as well as the properties of the first layer and the partial second layer.
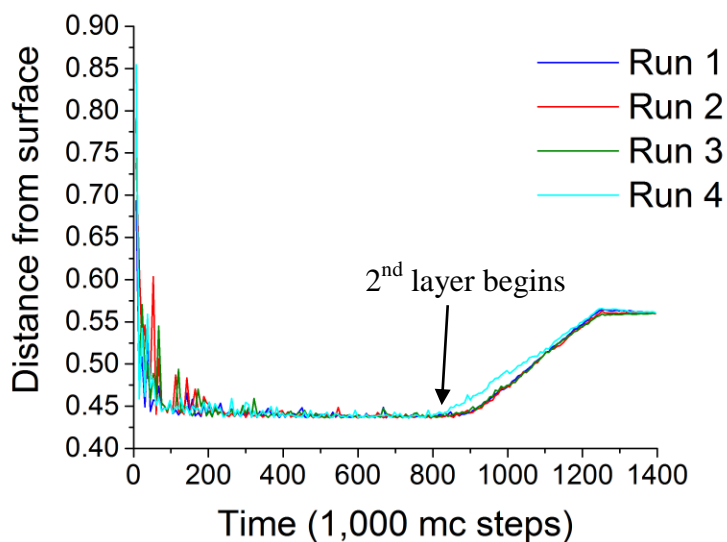
Figure 4.7 Average distance of chains from an adsorbing surface as a function of simulation time for four simulations of $N = 250$ chains in the medium sized box at $T_{red} = 1.5$. The increase in distance in the late part of the simulation indicates the formation of a second layer on the adsorbing surface.
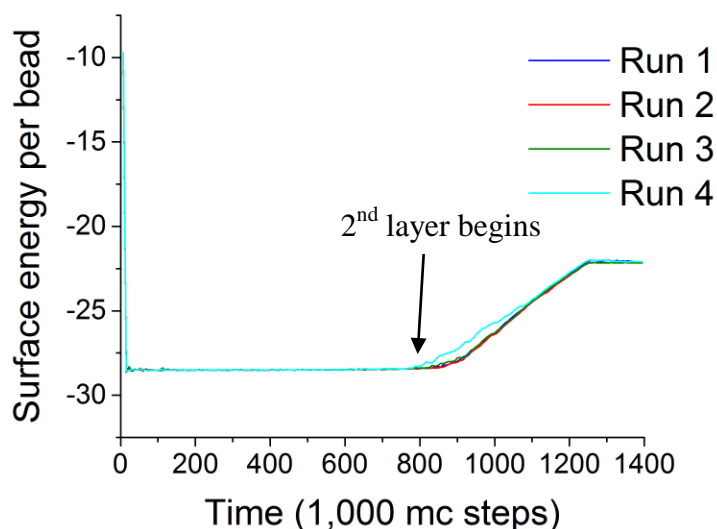
Figure 4.8 Surface energy per bead as a function of simulation time for four simulations of $N = 250$ chains in the medium size box at $T_{red} = 1.5$. The increase in surface energy in the late part of the simulation indicates the formation of a second layer on the adsorbing surfaces.

First, we look at the average surface potential energy and average surface distance as a function of time, shown in Figure 4.7 and Figure 4.8, respectively. The figures show results from four independent simulations, which agree well with each other. Early in the simulations, we see an

abrupt drop in distance from the surface and the surface energy per bead as the molecules begin forming the first layers on the substrates. At a time of about $8{\times}10^5$ MC steps, both the surface energy and distance begin to rise, which indicates that a second layer has begun to form. When all the molecules have entered the box and have been adsorbed, we see these graphs level off and become constant. Figure 4.9 shows a view of a final configuration that allows us to examine the first layer adsorbed to a surface. This layer is much more densely packed than the partial monolayer at the same temperature, $T_{\text{red}} = 1.5$, shown in Figure 4.6. The higher density in Figure 4.9 leads to the chains being less bent than in Figure 4.6, and the chains in the dense layer show much more orientational order than in the less populated layer.
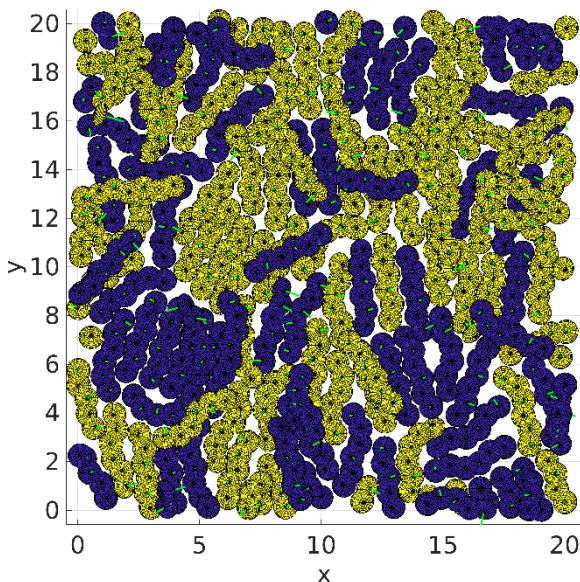
Figure 4.9 Top-down view of the adsorbed molecules on the ceiling of the box for a simulation of $N = 250$ chains in the medium box at $T_{\text{red}} = 1.5$. This view allows us to look through the ceiling at the first layer of adsorbed molecules.

We now take a deeper look at the layering characteristics of the final configurations. Figure 4.10 shows a side view of a final configuration, which illustrates the layering. We can clearly see that the formation of a second layer has begun on the floor and ceiling of the box for this simulation. In order to develop a better understanding of the process, we examine the probability distribution for the height (z-coordinate) of the beads shown in Figure 4.11. Each peak in this graph represents a distance from the bottom surface α-6T molecules are likely to be found. The strong peak at low height corresponds to the first adsorbed layer while the second highest peak

represents the second layer. The smaller peaks belong to chains that are part of both layers. By integrating the probability distributions for each peak over the height we can estimate the number of particles in each layer of the final configuration.
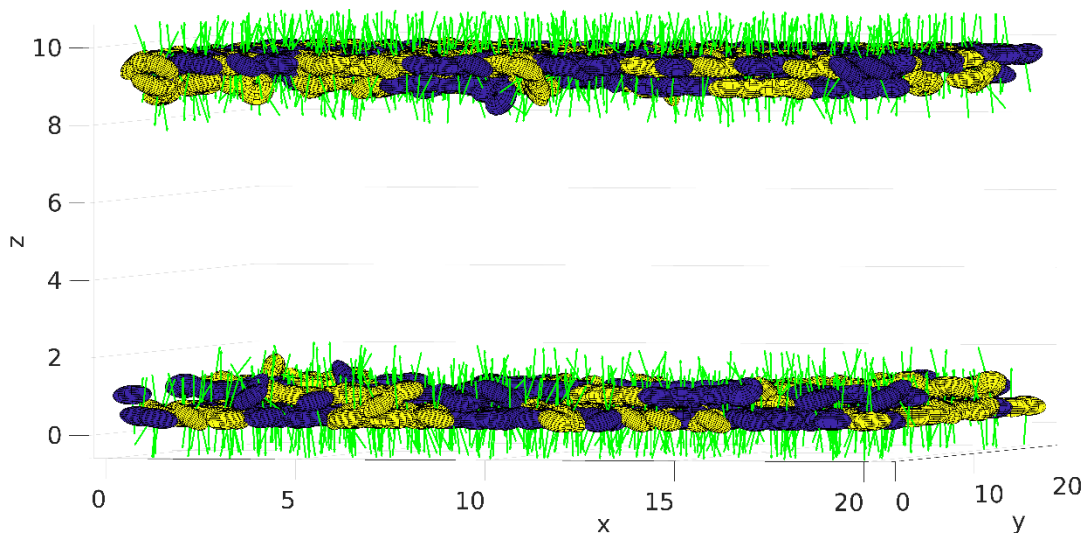
Figure 4.10 Final configuration for a simulation of $N = 250$ chains in the medium box at $T_{red} = 1.5$. This view highlights the presence of two layers on the floor and ceiling of the box.
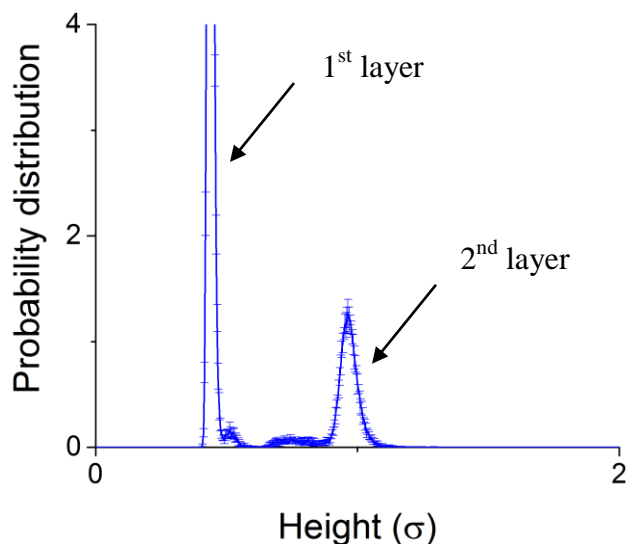
Figure 4.11 Probability distribution for the z-coordinate (height) of α-6T molecules deposited at $T_{red} = 1.5$ in the medium size box. Note that this graph shows the results near the bottom surface for only one of the simulations; the other simulations behave similarly. The probability distribution at the ceiling is nearly a mirror image of that at the floor for all simulations.

The average number of particles in the first layer for each adsorbing surface in our four simulations was found to be 95 ± 0.58. For the second layer, the average number of particles was found to be 30 ± 0.58. Furthermore, the average area densities for these layers were found to 0.235 ± 0.0014 chains/σ^2 and 0.0742 ± 0.0014 chains/σ^2. Thus for these simulations, the first layer is found to contain over three times as many molecules as the second, and it has a much higher area density, showing that the second layer is not complete.

4.3   Layer growth at low temperature

Finally, we investigate how layers grow at a low temperature of $T_{\mathrm{red}} = 0.75$. We performed simulations in our smallest box, $L_{\mathrm{x}} = 20.1\sigma_0$, $L_{\mathrm{y}} = 10.05\sigma_0$, and $L_{\mathrm{z}} = 10\sigma_0$, for chain numbers $N = 100$, 200, 300, and 400. For the case $N = 100$, the deposition rate was set to one new chain every 25,000 Monte Carlo steps. For all other cases, the rate was one new particle every 10,000 steps. For this part of the work, we are interested in the ordering of the first layer and the layering characteristics. The first layers of the final configurations for all simulations are shown in Figures 4.12 through 4.15.
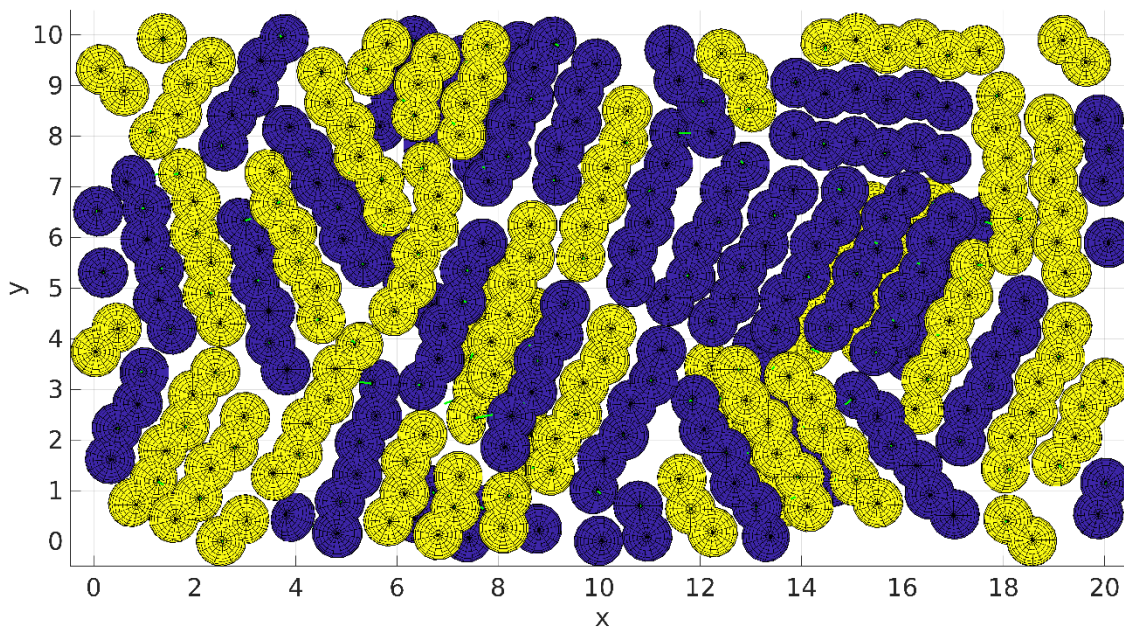
Figure 4.12 Top-down view of the first layer of molecules on the ceiling of the box for a simulation with $T_{\mathrm{red}} = 0.75$ and $N = 100$. Notice that the adsorbed layer has ordered regions with different orientations.
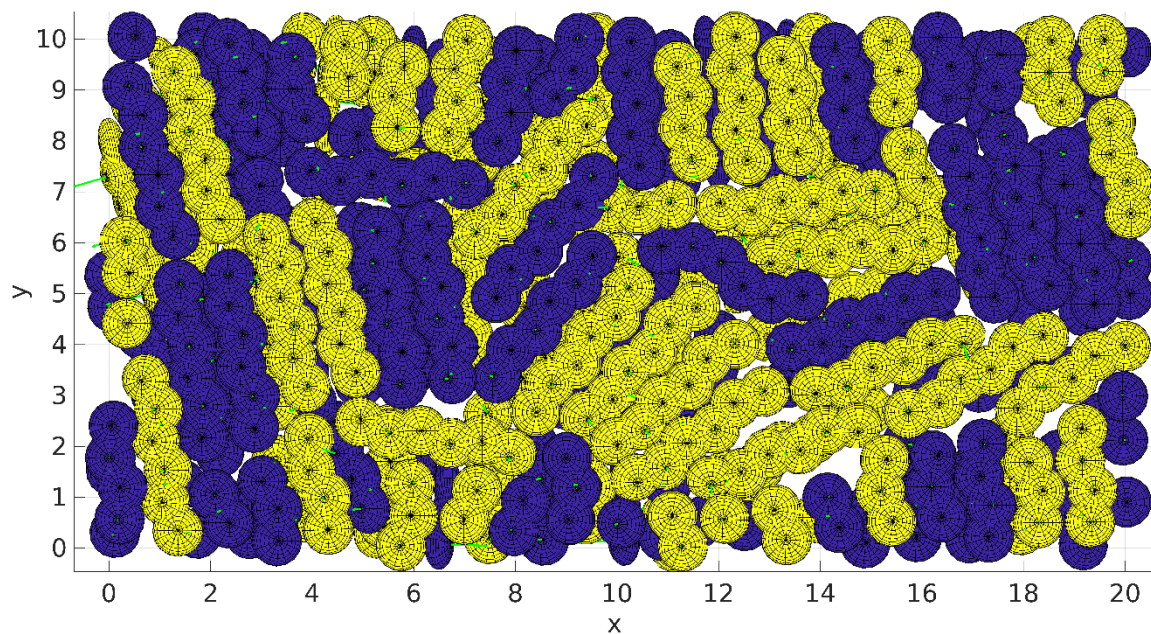
Figure 4.13 Top-down view of the first layer of molecules on the ceiling of the box for a simulation with $T_{red} = 0.75$ and $N = 200$. Notice that the adsorbed layer has ordered domains of different orientations.
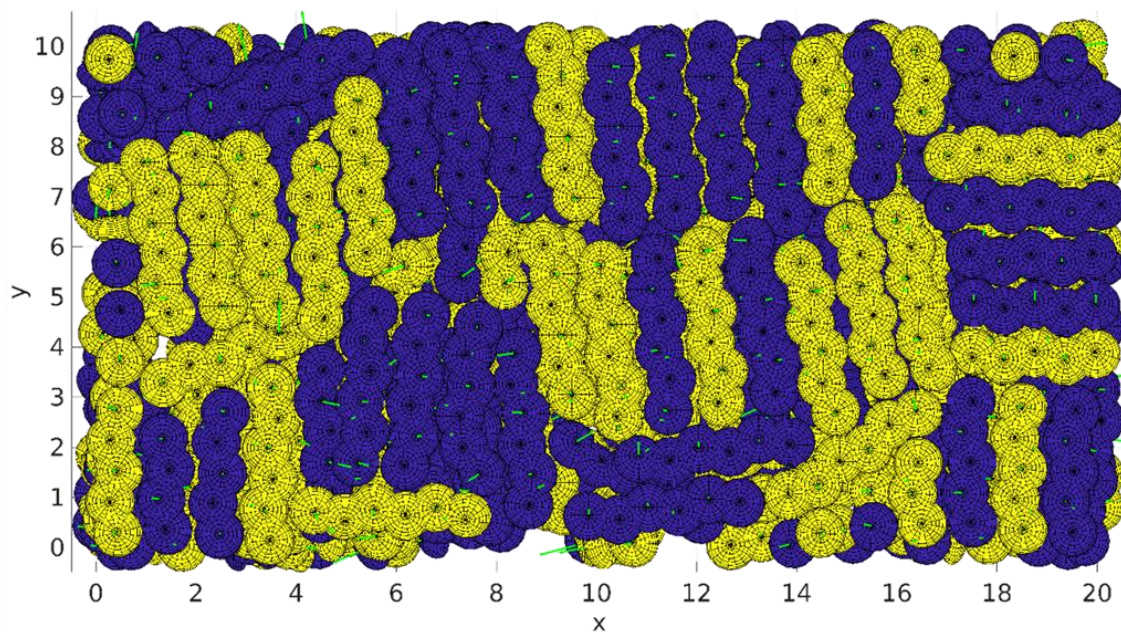
Figure 4.14 Top-down view of the first layer of molecules on the ceiling of the box for a simulation with $T_{red} = 0.75$ and $N = 300$. Notice that the adsorbed layer has highly ordered domains of different orientations.
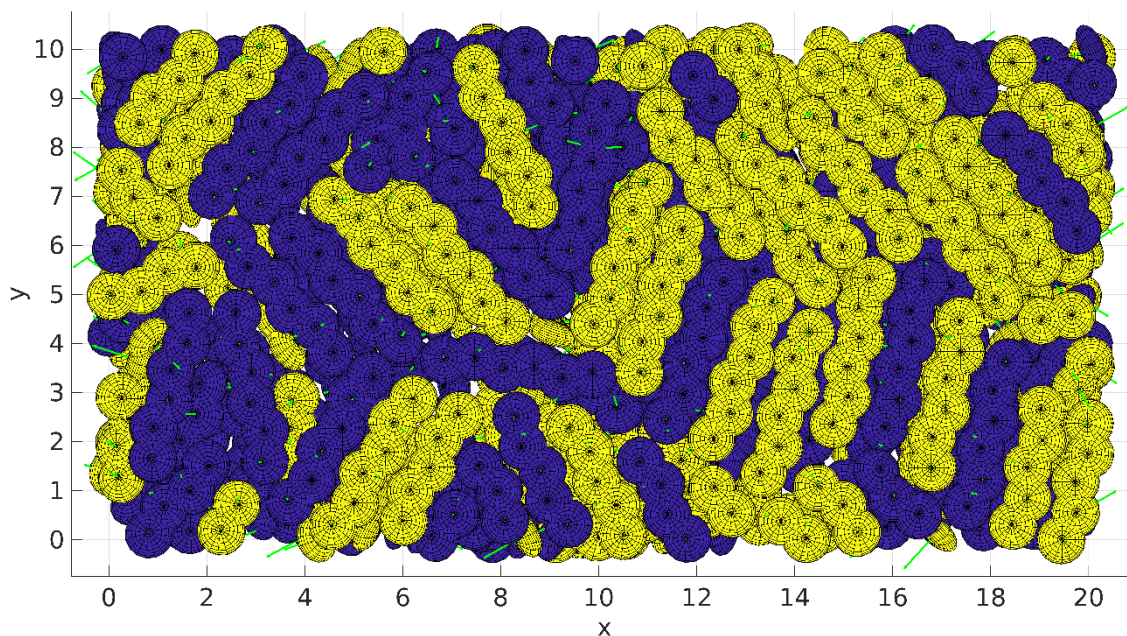
Figure 4.15 Top-down view of the first layer of molecules on the ceiling of the box for a simulation with $T_{red} = 0.75$ and $N = 400$. Notice that the adsorbed layer has ordered domains of different orientations.

We can clearly see that for the first layer in these simulations, the molecules form ordered domains as expected for this temperature. The final configurations for $N = 100$ and $N = 200$ show ordered regions separated by disordered areas. The final configurations for $N = 300$, on the other hand, shows a highly ordered domain that spans almost the entire area. The final configuration for $N = 400$ has dense, ordered domains with different orientations.

Now we examine the surface energy per bead and the average distance from a substrate as a function of simulation time. Results for all four simulations are presented in Figures 4.16 and 4.17 to better understand the layering behavior. For all simulations in this comparison, the surface energy drops to a minimum early in the simulations as the first layer begins to form. This drop is reflected in the average distance from the substrate, which is expected as the molecules are beginning to lie on the surfaces. Once enough molecules enter the box, we begin to see an increase in surface energy and distance from the substrate, which we associate with the formation of a second layer. For the $N = 100$ case, a small increase in surface energy and average distance from the substrate can be observed at around 2,500,000 MC steps. This is caused by a second layer beginning to form on the upper surface. The formation of the second layer for $N = 100$ starts later because the deposition rate is much smaller than in the other simulation. For the

24
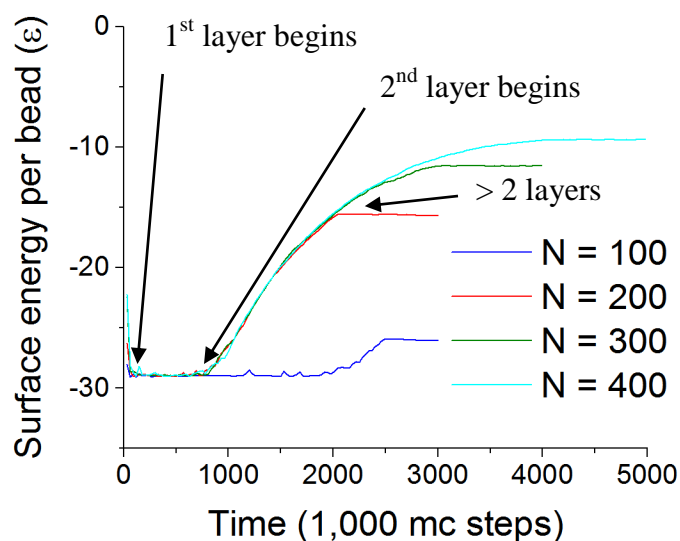
Figure 4.16 Surface energy per bead for simulations of 100 (blue), 200 (red), 300 (green), and 400 (cyan) molecules at $T_{red} = 0.75$ as a function of simulation time.
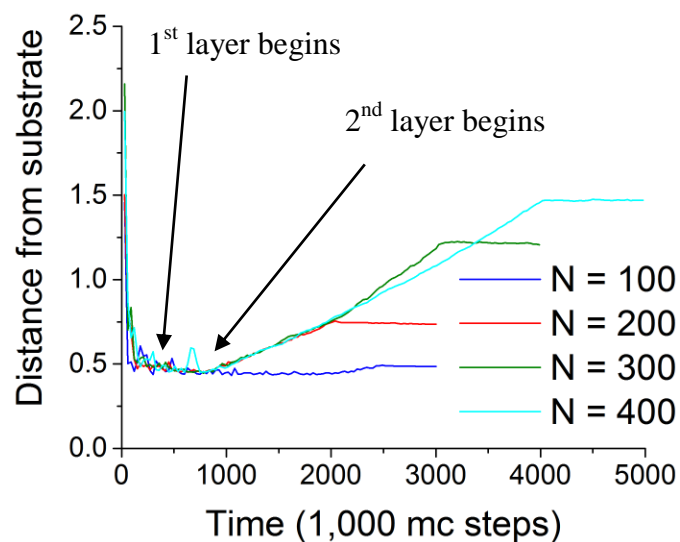
Figure 4.17 Average distance between molecules and the substrate as a function of simulation time. Simulation results for 100 (blue), 200 (red), 300 (green), and 400 (cyan) molecules at $T_{red} = 0.75$ are shown.

$N = 200$, 300, and 400 cases, we can see that the distance and energy both begin to increase at around 1,000,000 Monte Carlo steps. In the $N = 200$ case, this rise ends and the plots level off when a second layer is formed. For the $N = 300$ and $N = 400$ cases, the surface energy and average distance increases until all particles have been deposited, leveling off much more

gradually over time. The layering behavior for each of these simulations can be visualized in their final configurations, shown in side view in Figures 4.18 through 4.21. The probability distribution for *z*-coordinates of the beads (height) is presented in Figure 4.22. As in Section 4.2, it is important for determining molecular organization in the layers formed through deposition; results for layer densities are presented in Table 3.
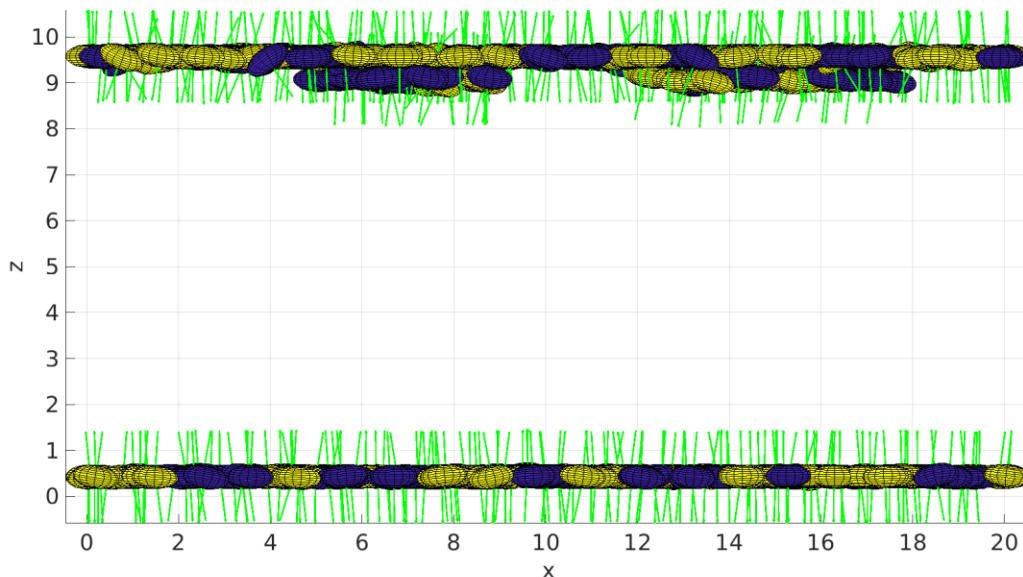
Figure 4.18 Final configuration for a simulation of $N = 100$ particles deposited at $T_{red} = 0.75$. A monolayer has formed at the bottom of the box, while at the top, the beginning of a second layer can be seen.

In the $N = 100$ case, we see that the molecules at the floor of the box form a monolayer which lies flat on the surface. At the ceiling, however, we see several molecules beginning to create the second layer. Integrating the probability distribution over the ranges of heights where the peaks form, we find that for this case there are approximately 44 molecules in each first layer, leaving approximately 12 molecules to form the second layer we observe. We find that the first layers for this graph have an area density of 0.218 molecules/σ^2, while the second layer has an area density of 0.057 molecules/σ^2.

26
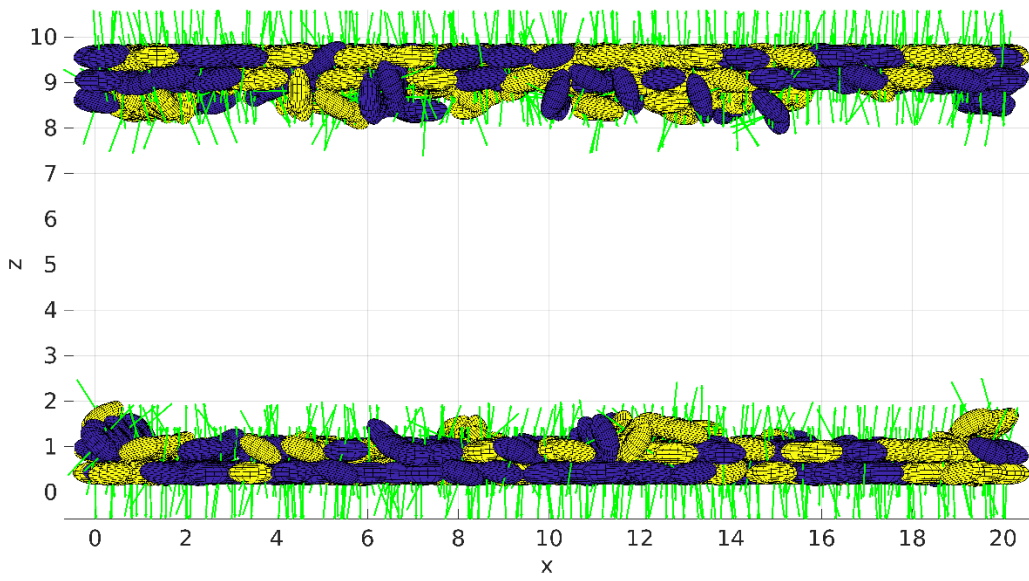
Figure 4.19 Final configuration for a simulation of $N = 200$ particles deposited at $T_{red} = 0.75$. This figure shows that two layers have formed at the floor and ceiling of the box, and molecules have begun piling onto the second layer.
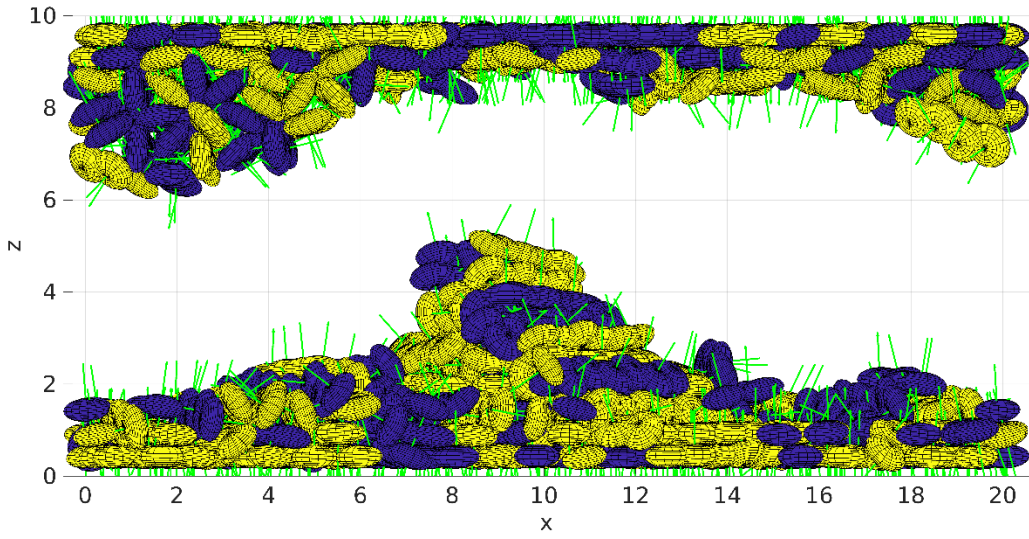
Figure 4.20 Final configuration for a simulation of $N = 300$ particles deposited at $T_{red} = 0.75$. This figure shows that two layers have formed at the floor and ceiling of the box, and molecules have formed large mounds or piles on top of these layers.
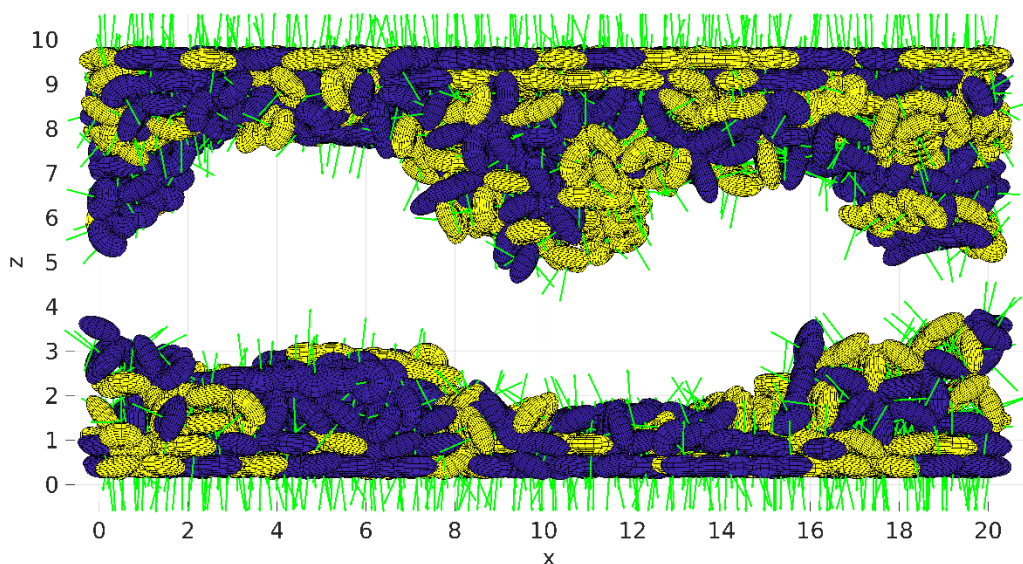
Figure 4.21 Final configuration for a simulation of $N = 400$ particles deposited at $T_{red} = 0.75$. As for the $N = 300$ case, after two layers, the molecules begin to form mounds or piles instead of new layers.
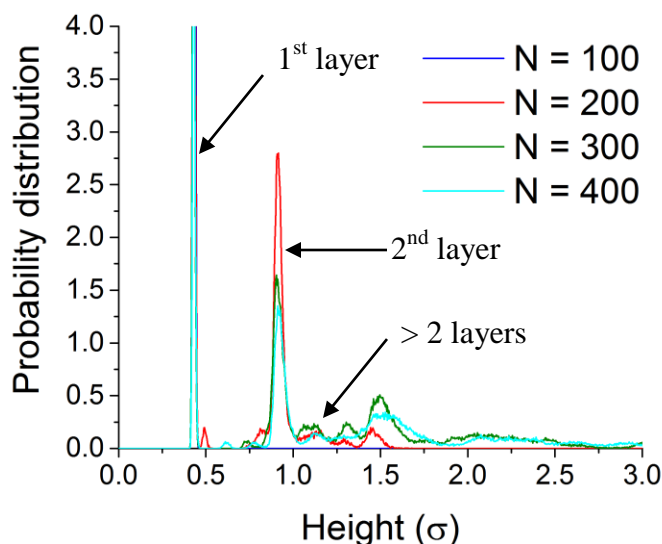
Figure 4.22 Probability distribution for the location of α-6T molecules deposited at $T_{red} = 0.5$ as a function of height in the box. Results for simulations of 100 (blue), 200 (red), 300 (green), and 400 (cyan) molecules are shown. This graph shows only the probability distribution for molecules near the lower surface.

For the $N = 200$ case, the number of molecules in each first layer is found to be approximately 43, while the number of molecules in each second layer is found to be approximately 40. This

tells us that approximately two full layers have been deposited on the floor and ceiling of the box, which is visually confirmed in Figure 4.19. Looking at this figure and the probability distribution, it is clear that some of the molecules in this configuration fall into the region between the two second layers. Approximately 27 molecules are present in this region for this configuration. The area densities of the first and second layers are found to be 0.212 molecules/ σ^2 and 0.198 molecules/ σ^2, respectively.

When the number of molecules increases to $N = 300$, the central region between the two layers at the floor and the two layers at the ceiling becomes much more disordered. The first layers are found to have approximately 48 molecules apiece, which is higher than in the 100 and 200 molecule cases. The second layers are found to hold approximately 37 molecules each. After this second layer, the piling of molecules creates a drastic increase in the number of molecules found in the central region. Approximately 131 molecules pile onto on another without forming layers, a phenomenon likely exacerbated by the proximity of the piles to where new molecules are injected. The area densities of the first two layers are found to be 0.235 molecules/ σ^2 and 0.182 molecules/ σ^2, respectively.

Similarly for the $N = 400$ case, the central region between top and bottom largely consists of piles of molecules on top of the lower two layers. The first layers consist of approximately 47 molecules with an area density of 0.230 molecules/ σ^2. The second layers contain approximately 42 molecules each, with an area density of 0.208 molecules/ σ^2. The central region contains over half of the deposited molecules at 223. As with the $N = 300$ case and confirmed in Figure 4.21, the molecules in this central region fail to form discernible layers.

T_{red}	Box size	N	Number of molecules in first layer	Number of molecules in second layer	First layer area density (chains/σ^2)	Second layer area density (chains/σ^2)
0.75	Small	100	44.2	11.6	0.218	0.057
0.75	Small	200	42.9	39.9	0.212	0.198
0.75	Small	300	47.5	36.9	0.235	0.183
0.75	Small	400	46.5	42.0	0.230	0.208
1.50	Medium	250	94.5	30.5	0.234	0.075
1.50	Medium	250	95.5	29.5	0.236	0.073
1.50	Medium	250	95.5	29.5	0.237	0.073
1.50	Medium	250	94.5	30.5	0.234	0.076

Table 3 Number of molecules per layer and area density for all simulations that produced more than a single monolayer in the final configuration.

Table 3 shows data for the number of molecules in the first two layers and the associated area densities for all simulations that produced more than one monolayer in their final configurations. From Table 3, we can see that, for $T_{red} = 0.75$, the first-layer area densities are very similar for $N = 100$ and $N = 200$. Indeed, the final configurations of these simulations presented in Figure 4.12 and Figure 4.13, also have about the same degree of order. For $N = 300$ and $N = 400$ at $T_{red} = 0.75$, the area densities are close to each other and greater than those for $N = 100$ or 200. This is confirmed by the denser, more ordered packing seen in the final configurations in Figure 4.14 and Figure 4.15. The first-layer area densities for $N = 300$ and $N = 400$ at $T_{red} = 0.75$ agree within the uncertainties with those of the high temperature simulations, $N = 250$ at $T_{red} = 1.5$. However, Figure 4.9 shows that the final configuration at the high temperature contains many bent molecules, which leads to less order than the straight rod chain conformations at the low temperature.

5   Summary and Conclusion

In this work, we investigated vapor deposition of rod-like molecules with Monte Carlo simulations of a coarse-grained model for α-sexithiophene (α-6T). Thiophenes are ring-shaped, π-conjugated molecules with applications in electronic devices. α-6T consists of six bonded thiophene rings. In the coarse-grained model, each ring is represented by a discotic ellipsoid (bead), whose orientation is described by a vector perpendicular to the plane of the disk. The α-6T molecule is modeled as a chain of six bonded, partly overlapping beads. The beads are connected to one another with bonds of fixed lengths and fixed bond angles. The orientation of neighboring beads along the chain is governed by a dihedral potential. A Gay-Berne potential describes interactions between beads in separate chains and a modified Gay-Berne potential describes the interactions between the beads and the substrate.

In the vapor deposition simulations, α-6T molecules are introduced, one at a time, into a simulation box with attractive, impenetrable surfaces as the floor and ceiling and periodic boundary conditions in the other two directions. Simulations were performed at low, intermediate, and high temperatures for varying particle numbers leading to coverages between sub-monolayer and several layers.

Simulations of sub-monolayers at different temperatures show positional and orientational order of the adsorbed molecules at low temperature, $T_{red} = 0.5$, orientational order at intermediate temperature, $T_{red} = 1.0$, and very little order at high temperature, $T_{red} = 1.5$. The shape of the single chains changes from straight rods at low temperature to bent chains at high temperatures. This is due to the dihedral potential, which keeps the orientation vectors of neighboring disks on the chain anti-aligned at low temperature.

Systems with a final coverage between one and two monolayers were simulated at high temperature, $T_{red} = 1.5$. We found a clear signature of the onset of formation of the second layer in both the surface energy and the average distance from the surface. The probability distribution for the z-coordinate (height) of the molecules showed a strong, narrow peak for the first layer and a weaker, broader peak for the second layer. The molecules in the first layer lie flat on the surface while those in the second layer assume a range of angles relative to the surface. The first layer is dense, has orientational order, and the molecules in the layer have bent conformations.

We studied layer growth at a low temperature, $T_{red} = 0.75$, with simulations for a range of deposited particles. Data for the surface energy and average height show a clear signature of the onset of growth of the second layer, however, the start of the third and fourth layer cannot be identified in this way. The probability distributions for the height show strong, narrow peaks for the first and second layer. At greater heights, we observe a number of small peaks suggesting that the molecules do not organize in layers beyond the second layer. This is confirmed by the final configurations, which show mounds of chains on top of the first two layers. This is probably a non-equilibrium effect. Longer simulation times after the last chains have been introduced are necessary to allow the system to relax to an equilibrium configuration. We should point out, however, that the experiments that inspired this work [6] were also conducted under non-equilibrium conditions.

A comparison of the first adsorbed layers of systems with more than one monolayer in the final state shows, that the area density is high in all cases. For deposition at low temperature, the first layer has domains with positional and orientational order. In contrast, deposition at high temperature leads to first layers with only orientational order.

6   Bibliography

[1] J. V. Selinger, Introduction to the Theory of Soft Matter, Springer, Switzerland, 2016.

[2] M. O'Neill and S. M. Kelly, "Liquid Crystals for Charge Transport, Luminescence, and Photonics," *Adv. Mater.,* vol. 15, pp. 1135-1146, 2003.

[3] I. McCulloch, M. Heeney, C. Bailey, K. Genevicius, I. Macdonald, M. Shkunov, D. Sparrowe, S. Tierney, R. Wagner, W. Zhang, M. L. Chabinyc, R. J. Kline, M. D. McGehee and M. F. Toney, "Liquid-Crystalline Semiconducting Polymers with High Charge-Carrier Mobility," *Nat. Mater.,* vol. 5, pp. 328-333, 2006.

[4] R. J. Kline, D. M. DeLongchamp, D. A. Fischer, E. K. Lin, M. Heeney, I. McCulloch and M. F. Toney, "Significant Dependence of Morphology and Charge Carrier Mobility on Substrate Surface Chemistry in High Performance Polythiophene Semiconductor Films," *Appl. Phys. Lett.,* vol. 90, pp. 062117-1-3, 2007.

[5] C. J. Garcia, "Investigation of single molecule and monolayer properties with Monte Carlo simulations of a coarse-grained model for a-sexithiophene," Master's Thesis, The University of Akron, Arkon, Ohio, USA, December 2017..

[6] A. Gujral, J. Gomez, J. Jiang, C. Huang, K. A. O'Hara, M. F. Toney, M. L. Chabinyc, L. Yu and M. D. Ediger, "Highly organized smectic-like packing in vapor-deposited glasses of a liquid crystal," *Chemistry of Materials,* vol. 29, pp. 849-858, 2017.

[7] A. Pizzirusso, M. Savini, L. Muccioli and C. Zannoni, "An atomistic simulation of the liquid-crystalline phases of sexithiophene," *J. Mater. Chem,* vol. 21, pp. 125-133, 2011.

[8] A. S. Almutairi., "Investigation of sexithiophene properties with Monte Carlo Simulations of a course-grained model," Master's Thesis, The University of Akron, Akron, Ohio, USA, December 2016.

[9] M. A. Bates and G. R. Luckhurst, "Computer simulation studies of anisotropic system. XXVI. Monte Carlo investigations of a Gay-Berne discotic at constant pressure," *J. Chem. Phys,* vol. 104, pp. 6696-6709, 1996.

[10] L. Bellier-Castella, D. Caprion and J. P. Ryckaert, "Surface ordering of diskotic liquid crystals," *J. Chem. Phys.,* vol. 121, pp. 4874-4883, 2004.